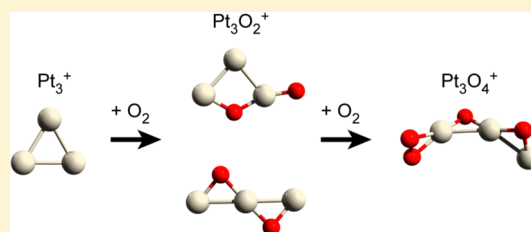


Structures of Platinum Oxide Clusters in the Gas Phase

Christian Kerpel,[†] Dan J. Harding,[†] Alexander C. Hermes,[‡] Gerard Meijer,[†] Stuart R. Mackenzie,^{*,‡} and André Fielicke^{*,†}[†]Fritz-Haber-Institut der Max-Planck-Gesellschaft, Faradayweg 4-6, D-14195 Berlin, Germany[‡]Department of Chemistry, University of Oxford, Physical and Theoretical Chemistry Laboratory, South Parks Road, Oxford, OX1 3QZ, U.K.

Supporting Information

ABSTRACT: The structures of small gas-phase $\text{Pt}_n\text{O}_{2m}^+$ ($n = 1-6$, $m = 1, 2$) cluster cations have been investigated in a combined infrared multiple photon dissociation (IRMPD) spectroscopy and density functional theory (DFT) study. On the basis of the infrared spectra obtained, it is concluded that in most clusters oxygen is bound dissociatively, preferring 2-fold bridge binding motifs, sometimes combined with singly coordinated terminal binding. Comparison of the oxide cluster structures with those of bare cationic platinum clusters reported previously reveals major structural changes induced in the platinum core upon oxygen binding. For some cluster sizes the presence of the Ar messenger atom(s) is found to induce a significant change in the observed cluster structure.



I. INTRODUCTION

Platinum plays an important role in heterogeneous redox catalysis showing versatile catalytic abilities including important industrial applications in car catalytic converters, in steam reforming, and in hydrogen based fuel cells.^{1,2} Whereas the aim in catalytic converters is to reduce the amount of harmful byproducts from burning fuel, steam reforming is used to activate C–H bonds to obtain valuable chemicals from cheap feedstocks like CH_4 . The key to platinum's importance in fuel cells lies in its ability to activate and dissociate molecular oxygen and several studies on different platinum surfaces have been undertaken, both experimentally (e.g., refs 3 and 4) and theoretically (for example, refs 5 and 6) to understand the details of this process. Despite the amount of work done in this area, many questions on the microscopic structures and reaction pathways remain open. One reason is the challenge in accurately treating platinum surfaces, even with state of the art theoretical methods, exemplified by the "CO on Pt(111) puzzle",^{7,8} where the wrong adsorption site preference for CO is predicted by certain quantum-chemical methods.

The chemistry of platinum clusters has been investigated in some detail. Strong size effects in reactivity and catalytic activity have been found for both deposited and gas-phase clusters, offering potential routes to tune the catalytic properties just by varying the particle size. The studies include the catalytic oxidation of CO to CO_2 on Pt clusters deposited on thin $\text{MgO}(100)$ films⁹ or in the gas phase.^{10,11} Other studies revealed a size dependence in the reactivity of charged Pt_n^\pm ($n = 1-21$) clusters in the gas phase with methane,^{12,13} other alkanes,¹⁴ and small molecules such as N_2O .¹⁵

To fully understand oxidation processes involving O or O_2 , a detailed knowledge of the platinum–oxygen chemistry is

necessary. On platinum surfaces a variety of molecular and atomic oxygen species have been described.^{3,4,16,17} Two types of molecular oxygen binding can be distinguished, namely superoxo (O_2^-) and peroxo (O_2^{2-}) species. In the first, a formal transfer of one electron into one of the antibonding π^* orbitals of the oxygen molecule occurs, leading to an activation of the O–O bond. As a result, the $\nu(\text{O}-\text{O})$ stretching frequency is red-shifted from the gas-phase O_2 value of 1580 cm^{-1} . Experiments have found superoxo species on Pt surfaces to show $\nu(\text{O}-\text{O})$ bands at 1250 cm^{-1} ,¹⁶ whereas other transition metal- O_2 complexes have superoxo stretches in the $1075-1195\text{ cm}^{-1}$ region.¹⁸ For peroxo species, frequencies for the O–O stretch on different Pt surfaces fall in the range $700-930\text{ cm}^{-1}$,¹⁶ where the higher activation is caused by the transfer of a second electron into an antibonding π^* orbital.^{3,16,18} However, in a matrix isolation experiment the antisymmetric stretch of the dioxide $\text{O}=\text{Pt}=\text{O}$ has been identified around 955 cm^{-1} .¹⁹ This may make a distinction between peroxo and terminal $\text{Pt}=\text{O}$ species difficult, if it is based solely on the experimental spectrum. For dissociated oxygen on surfaces, M–O stretches typically fall into the region between 480 cm^{-1} (hollow site binding³) and 560 cm^{-1} (bridge site binding¹⁷), but lower frequencies down to about 330 cm^{-1} for lateral vibrations of hollow site oxygen and higher frequencies up to 760 cm^{-1} for oxygen as subsurface "oxides" have also been reported.^{3,4}

Special Issue: Peter B. Armentrout Festschrift

Received: June 5, 2012

Revised: August 15, 2012

Published: August 15, 2012

In this study we have investigated $\text{Pt}_n\text{O}_{2m}^+$ clusters ($n = 1-6$; $m = 1, 2$) using infrared multiple photon dissociation (IR-MPD) spectroscopy of their argon complexes and determined their structure by comparison with DFT calculations.

II. METHODS

Experimental Section. The IR-MPD spectra were measured using a pulsed molecular beam experiment connected to a beamline of the Free Electron Laser for Infrared eXperiments (FELIX) facility²⁰ in The Netherlands and both the setup and the data analysis methods have been described in detail elsewhere.^{21,22}

Briefly, cationic platinum clusters are generated by laser ablation from an isotopically enriched ^{194}Pt target (96.4% enrichment, from Oak Ridge National Laboratory) in the presence of a pulse of carrier gas comprising 2% argon in helium. The resulting clusters, entrained in the gas pulse, pass through a reaction channel at room temperature, into which molecular oxygen is introduced via a second pulsed valve. In this channel, the clusters can react with O_2 and/or form complexes with Ar atoms. The resulting distribution expands into a vacuum, passing first through a skimmer and then through an aperture. Behind the aperture the cluster distribution is analyzed using a reflectron time-of-flight mass spectrometer.

Mass spectra are recorded alternately with and without FELIX irradiation. If the frequency of the IR beam is resonant with one of the IR active vibrations of a cluster complex, several photons can be absorbed sequentially and the resultant heating of the complex can lead to desorption of the argon atoms. Species that are dissociated following IR radiation have a lower intensity in the irradiated cluster beam compared to the reference distribution. Relative depletions are monitored as a function of the IR frequency, converted into cross sections,²³ and normalized according to the FELIX power, to yield the spectra shown below. Here, we have investigated the frequency range from 400 to 1420 cm^{-1} , which includes the typical fingerprint region for oxygen–oxygen and oxygen–metal vibrations. All spectra reported below show the raw data points together with a binomially weighted five point average.

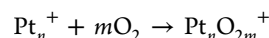
Theoretical Section. All calculations have been performed using density functional theory (DFT) as implemented in TURBOMOLE V6.2²⁴ together with the resolution of the identity (RI) approximation. The TPSS exchange–correlation functional²⁵ was used with the def2-TZVP basis sets for all atoms, and the def2-ecp effective core potential was used to treat the core electrons of Pt.^{26,27} This choice of functional and basis set has been found to give good descriptions of other similar systems that we have investigated recently, including bare and CH_4 ligated Pt_n^+ ($n = 3-5$) and Ta_nO_m^+ ($n = 6-11$, $m = 0-2$) clusters.^{13,28,29} For the smallest systems, containing only one or two platinum atoms, the number of possible binding geometries is limited. Therefore, no global optimization method was applied for these sizes, but a careful testing of possible structures has been performed including those found for neutral platinum oxides by Xu et al.³⁰ For all complexes with three or more platinum atoms basin hopping Monte Carlo simulation³¹ was used to identify low lying isomers at the PBE/def2-SVP level that were then reoptimized at the TPSS/def2-TZVP level.

For all structures different spin multiplicities ($2S + 1$) have been investigated, ranging from doublets to sextets in most cases. Where sextet states were found to be competitive in

energy, higher spin states have also been investigated. The calculated IR spectra are derived from analytical harmonic calculations, the frequencies are unscaled.

III. RESULTS AND DISCUSSION

General Remarks. In this study we focus on small platinum oxide clusters containing up to six Pt atoms. The oxides are formed by reaction of the preformed Pt cluster cations with molecular O_2 under thermalized conditions at ca. 30 °C in the reaction:



Therefore, clusters with an even number of oxygen atoms dominate the distribution.

We were able to record IR-MPD spectra of the dioxide clusters, Pt_nO_2^+ ($n = 1, 3, 6$) and the tetraoxides Pt_nO_4^+ ($n = 3, 5$). For Pt_2O_2^+ , Pt_4O_2^+ , and Pt_5O_2^+ we can only present the calculated structures and spectra to try to provide a more complete picture of the structural evolution with cluster size.

The messenger atom technique relies on the assumption that the messenger atom interacts only weakly with the cluster and does not perturb its structure; in many cases these assumptions are well founded but cases are known where the messenger has a significant influence.^{32,33} Here, most of the experimental spectra of the $\text{Pt}_n\text{O}_{2m}\text{Ar}^+$ complexes are compared to spectra calculated without inclusion of the Ar atom messenger(s) as they provide a satisfactory match to the experimental data. We see a significant influence of the messenger atoms for PtO_2^+ and Pt_3O_2^+ , for these species the spectra of complexes with two Ar atoms are also shown and the influence of the messenger atoms is investigated.

$\text{PtO}_2\text{Ar}_x^+$. The IR-MPD spectra of the cationic platinum dioxide complexes with one and two Ar atoms were recorded and the latter is shown in Figure 1 together with calculated spectra. The experimental spectrum of $\text{PtO}_2\text{Ar}_2^+$ exhibits a single band at 1200 cm^{-1} , a characteristic frequency for a superoxo unit. Neutral PtO_2 has been found to have a linear $\text{O}=\text{Pt}=\text{O}$ structure^{30,34} and the cationic ground state is predicted to have a similar, but slightly bent, geometry (isomer 1a). The most intense vibrational mode in the simulated

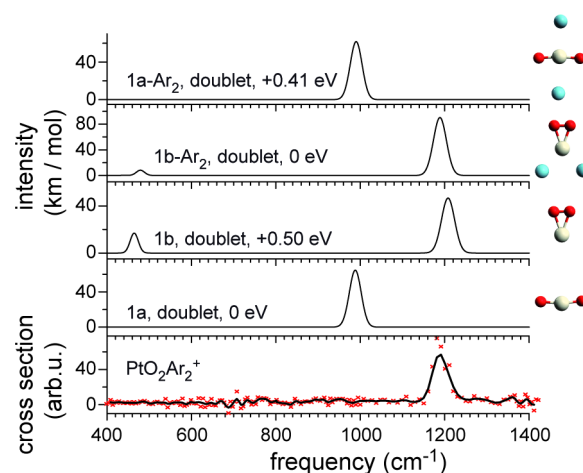


Figure 1. Experimental IR-MPD spectrum of $\text{PtO}_2\text{Ar}_2^+$ (bottom trace) together with the calculated spectra and structures of low lying isomers. The energies are given relative to the lowest energy isomer of PtO_2^+ and $\text{PtO}_2\text{Ar}_2^+$, respectively. The platinum atoms are shown in white, the oxygen in red, and argon in blue.

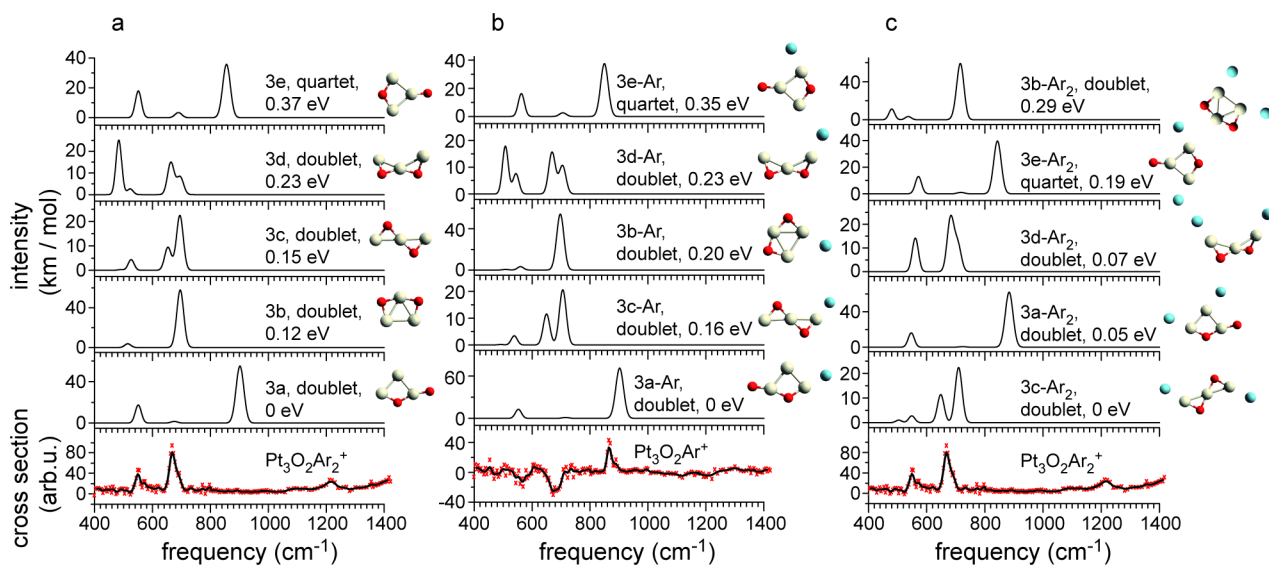


Figure 2. Experimental spectra for $\text{Pt}_3\text{O}_2\text{Ar}_2^+$ and $\text{Pt}_3\text{O}_2\text{Ar}^+$ and calculated spectra for low lying isomers of Pt_3O_2^+ (a), $\text{Pt}_3\text{O}_2\text{Ar}^+$ (b), and $\text{Pt}_3\text{O}_2\text{Ar}_2^+$ (c).

spectrum of this isomer is at 990 cm^{-1} , significantly different from the experimental band position.

An isomer containing a superoxo unit, **1b**, has been identified 0.5 eV above isomer **1a**. The band dominating the simulated IR spectrum of isomer **1b** matches the experimental finding well (though the weak calculated band at 450 cm^{-1} is not visible in our experiment), suggesting the presence of a high-energy, metastable isomer of PtO_2^+ in our cluster beam. This is somewhat surprising until the effect of the Ar atoms is explicitly included in the calculations. The energetic order of the isomers is then reversed and the $\text{PtO}_2\text{Ar}_2^+$ complex with molecularly bound O_2 , **1b-Ar₂**, becomes favored by 0.41 eV (Figure 1). Additionally, the relative intensities of the bands at 1200 and 450 cm^{-1} change, making the band at 450 cm^{-1} less prominent. It is not, however, clear if the bare PtO_2^+ clusters in our beam have the $\text{O}=\text{Pt}=\text{O}$ structure or if they bind O_2 molecularly, remaining kinetically trapped behind a large barrier to O_2 dissociation.

The experimental spectrum of PtO_2Ar^+ is very similar to that of $\text{PtO}_2\text{Ar}_2^+$ (Supporting Information). In PtO_2Ar^+ the calculations predict the two isomers to be essentially isoenergetic with the calculated spectrum of the molecularly bound species matching the experimental spectrum well (Supporting Information). Interestingly, although significant changes in the relative energies are predicted, the calculated spectra of the two PtO_2^+ isomers change little on Ar binding. Small shifts in band positions and intensities are calculated, but the main spectral features at 1000 and 1200 cm^{-1} remain essentially unchanged.

Pt₃O₂Ar_x⁺. For this cluster size spectra were also obtained for complexes with one and two Ar atoms. However, the spectrum measured in the $\text{Pt}_3\text{O}_2\text{Ar}^+$ channel was significantly perturbed by dissociation products (Ar loss) from $\text{Pt}_3\text{O}_2\text{Ar}_2^+$. Therefore, the latter species is discussed first. Three main features are visible in the experimental spectrum of $\text{Pt}_3\text{O}_2\text{Ar}_2^+$, one weak band at about 1220 cm^{-1} , and two stronger ones at 550 and 680 cm^{-1} (Figure 2a). The lowest energy structure (**3a**) found for Pt_3O_2^+ contains a triangular Pt_3^+ unit, similar to the structure found for the bare metal cluster,²⁸ but the IR spectrum does not match the experiment well. This isomer

contains a terminal $\text{Pt}=\text{O}$ unit and a bridging O atom. The next three structures (which are all close in energy) contain two O bridges and their spectra fit reasonably, except for the band at 1220 cm^{-1} in the experimental spectrum. Given that this frequency is characteristic for a superoxo O_2^- group and that the lowest lying molecularly bound species are more than 1 eV higher in energy than the dissociated structures the most likely explanation for it is a kinetically trapped species in the beam. The highest energy isomer (**3e**) shown in Figure 2a is very similar to isomer **3a** but has the terminal O bound to a different Pt atom.

The experimental spectrum of the $\text{Pt}_3\text{O}_2\text{Ar}^+$ species (Figure 2b) is affected by the fragmentation of $\text{Pt}_3\text{O}_2\text{Ar}_2^+$, leading to the dips at 550 and 680 cm^{-1} . Whereas absorption bands in these regions would be difficult to observe, there is a band at 880 cm^{-1} , a mode not observed for $\text{Pt}_3\text{O}_2\text{Ar}_2^+$. This band is almost exactly at the position of the most intense band predicted for the lowest-energy structure of Pt_3O_2^+ **3a**.

Panels b and c of Figure 2 show the effects of the explicit inclusion of argon atoms in the calculations. Inclusion of a single argon atom still leads to the same lowest energy structure as the bare cluster. For the other isomers the energy ordering is slightly altered, but overall there is little change in the predicted IR spectra. For the complex with two Ar atoms the double (trans) O bridged quasi-linear isomer (**3c-Ar₂**) is the lowest energy calculated structure with isomer **3a-Ar₂** and **3d-Ar₂** practically isoenergetic. Clearly, **3c-Ar₂** and **3d-Ar₂** yield vibrational spectra that match the experiment better than **3a-Ar₂**. They lack the $\text{Pt}=\text{O}$ group, which leads to the prominent peak at 880 cm^{-1} in $\text{Pt}_3\text{O}_2\text{Ar}^+$.

The change in the energetic ordering upon Ar attachment is a direct consequence of different Ar binding energies. For all isomers except **3b**, the calculated binding energy of the first argon atom differs only slightly (between 0.55 and 0.57 eV , 0.47 eV for **3b**). In contrast, the binding energy of the second argon varies significantly: **3c-Ar**, **3d-Ar**, and **3e-Ar** have similar binding energies for the second argon compared to the first one (0.53 , 0.52 , and 0.53 eV , respectively), whereas **3a-Ar** and **3b-Ar** have significantly weaker binding (0.32 and 0.28 eV , respectively).

The most important contribution to the Ar bonding is likely to be charge induced dipole interactions and, therefore, the DFT calculations can be expected to capture the most important bonding contributions. We have undertaken test calculations to assess possible contribution of basis set superposition errors to the argon binding energies, using the counterpoise correction. We find the binding energies change by less than 0.04 eV, significantly smaller than the difference in energy for the two argon binding sites of **3a-Ar₂**.

A natural population analysis of the isomers **3a-Ar₂**, **3c-Ar₂**, and **3d-Ar₂** shows that the weaker bound Ar atom in **3a-Ar₂** (partial charge 0.12 e) is attached to a platinum atom with partial charge of 0.2 e (Figure 3). In contrast, the stronger

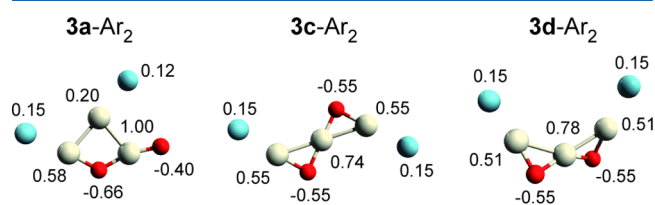


Figure 3. Partial atomic charges for three isomers of $\text{Pt}_3\text{O}_2\text{Ar}_2^+$ derived from natural population analysis.

bound Ar atom of **3a-Ar₂** and both the Ar atoms of **3c-Ar₂**, and **3d-Ar₂**, have 0.15 e partial charge and are found at Pt atoms with significantly higher partial charges (0.51–0.58 e). This is consistent with their higher binding energies and leads to a change in the energetic order of the Pt_3O_2^+ isomers in the diargon complex. The strongly charged third platinum atom (+1.00 e) in **3a-Ar₂** appears to be a more attractive binding site for the argon atom. However, the two adjacent oxygen atoms are negatively charged with a charge sum of -1.06 e and are evidently effective in shielding the positive charge.

Pt₃O₄Ar⁺. The spectrum of $\text{Pt}_3\text{O}_4\text{Ar}^+$ (Figure 4) is very similar to that of $\text{Pt}_3\text{O}_2\text{Ar}_2^+$ (Figure 2a). Again, three bands are visible at ca. 550, 700, and 1190 cm^{-1} , almost identical positions to those observed for the dioxide. However, the high frequency (superoxo) band is more pronounced. Two of the

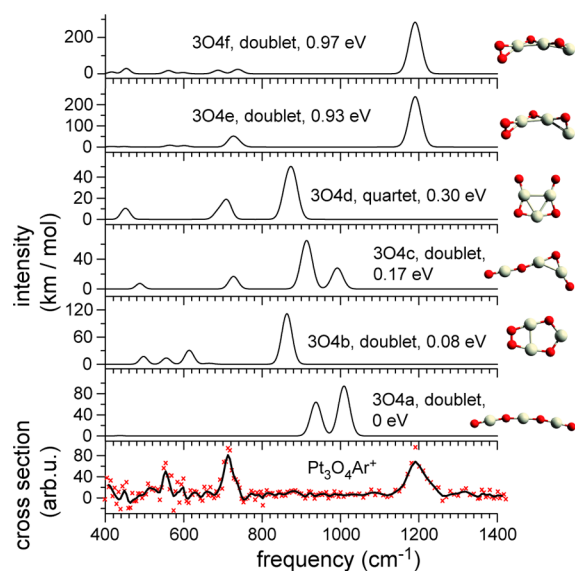


Figure 4. Experimental spectrum of $\text{Pt}_3\text{O}_4\text{Ar}^+$ and the calculated spectra of low lying isomers of Pt_3O_4^+ .

four low-lying isomers, **3O4a** and **3O4c**, contain nearly linear Pt–O–Pt units. Along with isomer **2a** of Pt_2O_2^+ (see below), these are the only cases of such a structural motif we have found. Xu et al. report similar motifs in the low energy isomers of small neutral Pt_nO_{2n} clusters, particularly for Pt_5O_{10} .³⁰ Most clusters considered in our study have lower relative oxygen content and, therefore, retain a significant amount of direct Pt–Pt bonding.

The spectra of the lowest-energy isomers (**3O4a–d**) are poor matches to the experiment whereas the calculated band positions of isomers **3O4e** and **3O4f** agree reasonably well with the experimental spectrum, despite their calculated structures lying nearly 1 eV above the lowest energy isomer. Therefore, the latter two isomers are the most likely candidates for the species observed in the beam. The fact that the other species are not observed, although they are significantly more favorable in energy, is probably related to the growth mechanism of the complex. Significant rearrangement of any low lying Pt_3O_2^+ complex is necessary upon binding of the second oxygen molecule to form isomer **3O4a** or **3O4c**. The situation is less clear for **3O4b** and **3O4d**, because low lying isomers exist for Pt_3O_2^+ that have similar structures, from which these complexes could conceivably be formed. One possible explanation is that the $\text{Pt}_3\text{O}_4\text{Ar}^+$ complex grows directly from the diargon complexes, **3c-Ar₂** or **3d-Ar₂**, of $\text{Pt}_3\text{O}_2\text{Ar}_2^+$ via Ar/O₂ ligand exchange, leading to the isomers **3O4f** and **3O4e**, respectively. The heat of adsorption could be removed by the desorbing argon atom, leaving a species kinetically trapped in a high energy configuration. Such kinetic trapping due to ligand exchange has recently been reported in the case of CH₄ adsorption on small cationic platinum clusters, where an early reaction intermediate was stabilized in the entrance channel.¹³

To further clarify the situation, calculations including the argon atom have been undertaken, in which we found that the binding energies of argon differ significantly for the Pt_3O_4^+ isomers. **3O4a** and **3O4c** bind Ar by only 0.06 and 0.03 eV, respectively. As the experiment was carried out at room temperature, these argon complexes are unlikely to survive in the beam, even if these isomers contribute significantly to the Pt_3O_4^+ mass peak. **3O4e** and **3O4f** bind the argon most strongly (0.54 and 0.56 eV, respectively), followed by **3O4d** (0.39 eV) and **3O4b** (0.35 eV). The latter two argon complexes are still more than 0.5 eV lower in energy than the **3O4e** argon complex, but it appears that the **3O4e** and/or **3O4f** argon complexes are favored due to their formation mechanism and the stronger binding of the argon atoms.

Pt₂O₂⁺, Pt₄O₂⁺, and Pt₅O₂⁺. Unfortunately, no interpretable experimental spectra were obtained for Pt_2O_2^+ , Pt_4O_2^+ , and Pt_5O_2^+ , although argon complexes of these species are detectable in the mass spectrum. Possible explanations could be that the IR absorption cross sections for these systems are very low, that the argon is so strongly bound that we can not dissociate the complex, or that upon absorption of a small number of photons the cluster rearranges into another structure and stops absorbing. However, our calculations find neither especially low IR intensities nor unusually high Ar binding energies for the identified low lying isomers. Given the success of the calculations for the other cluster sizes so far, we have investigated possible structures using DFT basin-hopping to obtain a more complete picture for the size-dependent structural evolution of the Pt_nO_2^+ species.

The lowest lying calculated isomers for Pt_2O_2^+ can be seen in Figure 5a. Isomer **2a** is an almost linear O–Pt–O–Pt chain,

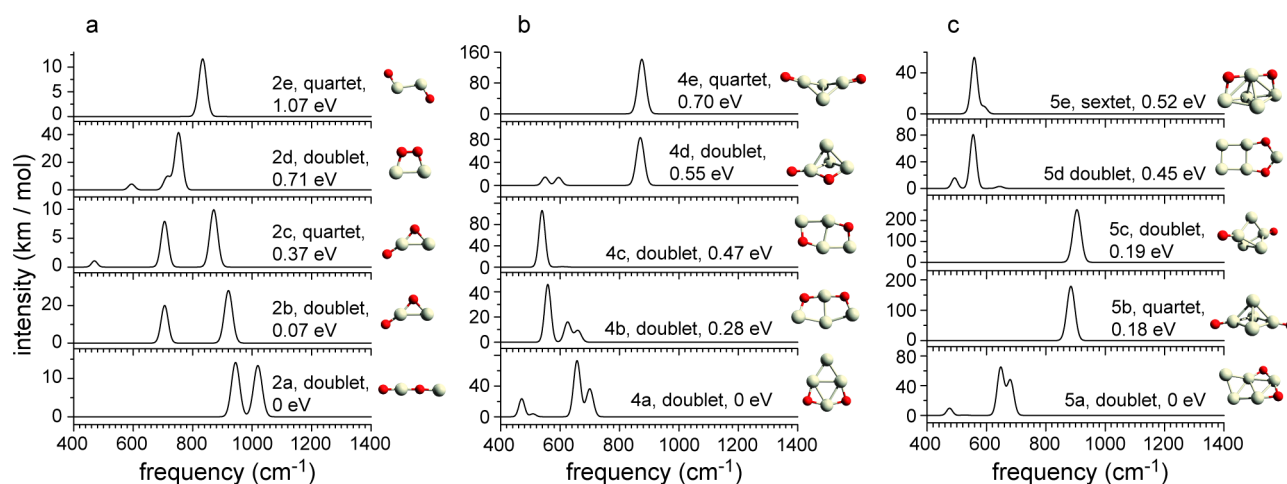


Figure 5. Calculated spectra and structures for Pt_2O_2^+ (a), Pt_4O_2^+ (b), and Pt_5O_2^+ (c).

whereas the nearly isoenergetic structure **2b** (+0.07 eV) contains a Pt–Pt unit with one bridging and one terminal oxygen atom. Similar structures have been reported as the lowest energy isomers for neutral Pt_2O_2 but with a significantly larger energy gap favoring the Pt–Pt chain structures for the neutrals.³⁰ Again low spin state isomers seem to be energetically preferred as shown in the comparison of **2b** and **2c** that are separated by as much as 0.3 eV. Isomer **2d** represents the lowest energy structure of a molecularly bound (O_2^{2-}) species with a main spectral feature around 750 cm^{-1} , whereas **2e** consist of a Pt–Pt chain with two terminal oxygen atoms.

Figure 5b shows the lowest energy structures found for Pt_4O_2^+ and their predicted IR spectra. Isomer **4a** has an almost planar rhombic Pt_4 structure with two O bridges and is clearly favored in energy. The next lowest energy structures we found, **4b** and **4c**, are also relatively flat and contain bridge-bound O atoms. Both isomers were found from starting structures based on tetrahedral Pt_4 units which collapsed during optimization. Structures **4d** and **4e** are considerably higher in energy, probably due to the presence of terminal O atoms. For comparison, far-IR-MPD spectroscopy has found Pt_4^+ to have a tetrahedral structure²⁸—nevertheless, different theoretical studies predict rhombic and tetrahedral $\text{Pt}_4^{+/0}$ to be close in energy.^{35,36} It appears that oxidation of these small Pt clusters leads to more planar structures, favoring the flat structures **4a–c** over the more three-dimensional structures **4d** and **4e**. The prediction of a distorted 2D square with 4 bridging oxygen atoms as the lowest energy structure of neutral Pt_4O_4 fits well into this picture.³⁰

For Pt_5O_2^+ we find a putative ground state structure very similar to the lowest lying structure found for Pt_4O_2^+ (**5a** in Figure 5c). The additional platinum atom adds to one edge of the rhombus and is slightly bent out of its plane. The higher lying isomers **5b**, **5c**, and **5e** are based on more or less strongly distorted trigonal bipyramidal Pt_5 cores. As in the case of Pt_4O_2^+ , the two lowest lying structures with a 3D Pt core have terminal bound oxygen atoms. One nearly planar structure, **5d**, is among the low lying isomers. Comparison with the bare metal clusters yields a similar picture compared to Pt_4O_2^+ . Pt_5^+ forms a trigonal bipyramid,²⁸ but theoretical studies for both cationic and neutral clusters predict a competition with planar structures.^{35,36} The lowest energy structure found by Xu et al. for neutral Pt_5O_5 is an almost planar pentagon with five bridging oxygen atoms, of which three are bent out of plane.³⁰

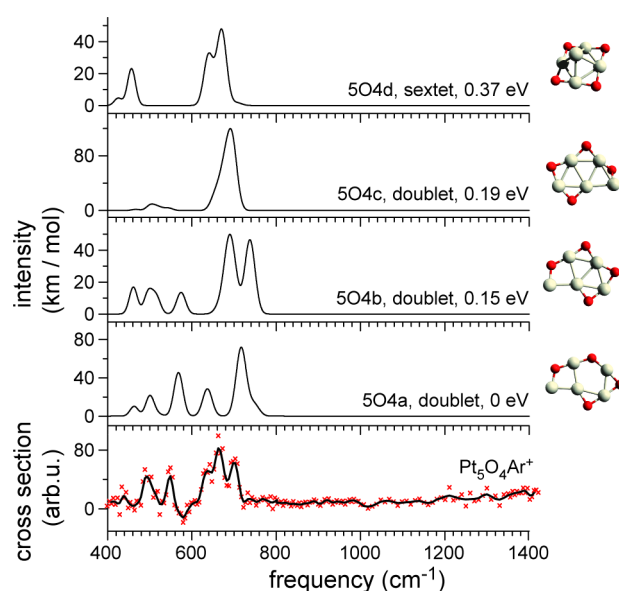


Figure 6. Calculated spectra for Pt_5O_4^+ and experimental spectrum for $\text{Pt}_5\text{O}_4\text{Ar}^+$.

$\text{Pt}_5\text{O}_4\text{Ar}^+$. The spectrum of $\text{Pt}_5\text{O}_4\text{Ar}^+$, shown in Figure 6, is more complicated than the other spectra presented so far. Bands are only visible between 400 and 700 cm^{-1} and in contrast to Pt_3O_4^+ there is no sign for the presence of a superoxo mode around 1200 cm^{-1} . The three lowest lying isomers (**5O4a–c**) have very similar structures, all containing a trapezoidal arrangement of the five Pt atoms and in **5O4c**, one of the O bridges points out of the plane of the cluster. The lowest energy structure with a 3D arrangement of the platinum atoms, i.e., a square pyramid, is about 0.37 eV higher in energy (**5O4d**). It contains four bridge-bound oxygen atoms surrounding the pyramid's base and has a sextet electronic state. The calculated spectra of the different isomers of Pt_5O_4^+ are rather similar and resemble the experimental one, with the two lowest-energy structures providing the best matches. All the isomers are relatively close in energy, and due to the similarity of their spectra, it is not possible to determine if all are present in the beam or if one isomer dominates. However, isomers **5O4a** and **5O4b** could explain all of the features visible in the experimental spectrum and are based on the lowest energy isomer we have found for Pt_5O_2^+ . Calculations

performed on the Ar complexes show only minor changes both for the relative energies of the two lowest isomers and for their spectra.

Pt_6O_2^+ . $\text{Pt}_6\text{O}_2\text{Ar}^+$ is the largest cluster for which a clear experimental spectrum has been obtained (Figure 7). Two

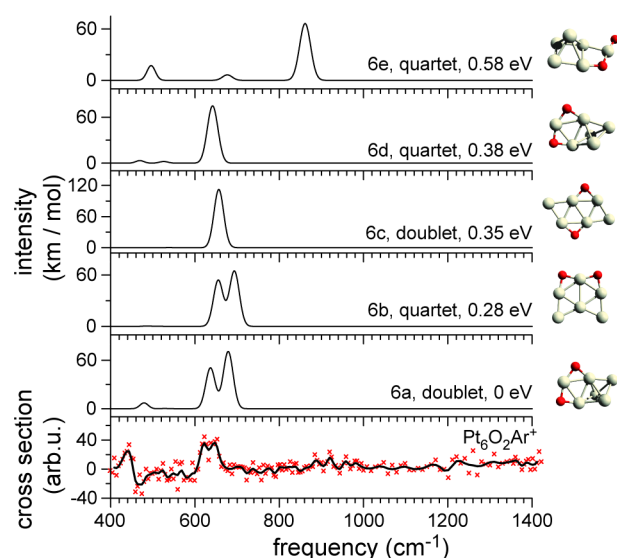


Figure 7. Calculated spectra for Pt_6O_2^+ and experimental spectrum for $\text{Pt}_6\text{O}_2\text{Ar}^+$.

absorption features are visible, one at about 440 cm^{-1} and a second, which appears to be split, at around 650 cm^{-1} . Isomers **6a** to **6d** all show bands in the $600\text{--}700\text{ cm}^{-1}$ region, which can be related to their O bridge structural motifs. The calculated spectra are all rather similar, though in **6a** and **6b** the Pt–O stretching modes are split. Whereas all calculated spectra agree well with the observed bands at around 650 cm^{-1} , the strong intensity of the band around 440 cm^{-1} in the experimental spectrum is not well matched in the calculated spectra with a weak band around 480 cm^{-1} only visible for **6a** and **6d**. As isomer **6a** is clearly favored in energy, it can be assumed to be the dominant species in the cluster beam.

IV. CONCLUSION

On extended Pt surfaces oxygen binding is well-known to induce substantial surface reconstructions.³⁷ Our observation of significant oxygen-induced structural changes in the metal frameworks of the $\text{Pt}_n\text{O}_{2m}^+$ clusters compared to the bare Pt_n^+ clusters²⁸ is consistent with this. For example, for the metal framework of Pt_3O_4^+ we observe a change from the trigonal bipyramid of the bare metal cluster to a planar structure. The $\text{Pt}_3\text{O}_2\text{Ar}^+$ species has a Pt–O–Pt bridge type insertion into the triangular metal cluster, whereas for Pt_3O_4^+ the three platinum atoms form a chain rather than a triangle. Overall, the binding of oxygen atoms tends to lead to flatter structures, with Pt_4O_2^+ and $\text{Pt}_5\text{O}_{2m}^+$ ($m = 1, 2$) favoring planar structures over the 3D structures observed for the bare clusters. Given this oxidation induced change in structure, it might be more appropriate to speak of the formation of platinum oxide clusters when referring to small Pt_nO_{2m} species instead of platinum clusters with oxygen adsorbates.

On Pt(111) oxygen molecules adsorb dissociatively via molecular intermediates that can be stabilized at low temperatures,³⁸ finally forming a $p(2\times 2)$ adlayer³⁹ with O atoms in 3-

fold hollow sites. On other Pt surfaces dissociative binding is also observed, usually leading to O in high coordination sites such as 3-fold binding on both (110) and (310) microfacets on Pt(210). Cases of bridging oxygen atoms have also been found but are rare.⁴⁰ In contrast, the bridging motif is by far the most prominent binding motif on the clusters examined in this work, being present in all of the oxides (except on the atom). Additionally, we found some cases where terminal bound oxygen atoms are present, especially for Pt_3O_2^+ , which are not observed for surfaces. As mentioned above, oxygen adsorbs dissociatively on Pt surfaces, but molecularly bound precursors can be stabilized at low temperatures, a situation that seems to be matched by our results. We only observe significant fractions of complexes with molecularly bound oxygen when the number of oxygen atoms exceeds the number of Pt atoms. In the case of PtO_2^+ the molecularly bound species seems to be stabilized by the attached argon, whereas the molecularly bound species for Pt_3O_4^+ appears to be a kinetically trapped species. Another example for a molecularly bound species is Pt_2O_4^+ . Here, an interpretable experimental spectrum is only obtained above 800 cm^{-1} ; however, a band at 1220 cm^{-1} can be unambiguously assigned to a superoxo species (Supporting Information).

It is also interesting to compare our results to those for Ta_nO_m^+ clusters ($n = 6\text{--}11$; $m = 0\text{--}2$).²⁹ As for platinum surfaces, oxygen binds dissociatively to tantalum surfaces with molecularly bound species as intermediates (ref 41 and references therein) and prefers high coordination binding sites.⁴² The investigations of the clusters revealed 2-fold bridge binding to be preferred for all oxide species. Concerning induced structural changes, the tantalum oxides behave differently to the platinum clusters: Upon oxygen binding, no major structural rearrangements were observed. This is probably related to the stronger Ta–Ta bonds, which are also reflected in bulk properties like significant higher melting temperature or enthalpy of vaporization of tantalum compared to platinum.⁴³

The insights into the structural changes of the platinum core upon oxygen binding and the knowledge of the preferred binding geometries obtained in this study provide important information for future studies of oxidation reactions on small platinum clusters. First, we have found that a relatively inexpensive theoretical approach seems to be sufficient to describe the interaction of platinum clusters with oxygen ligands and second, the oxide structures found here may be relevant in catalytic oxidation reactions. The changes induced in the structures of the platinum core upon the oxygen binding may be particularly important, as similar local changes may need to be considered for low coverage reactions on surfaces, larger clusters, and deposited clusters to determine the intermediate steps of oxidation reaction mechanisms.⁴⁴

■ ASSOCIATED CONTENT

Supporting Information

Experimental spectrum and calculated spectra of PtO_2Ar^+ . Experimental spectrum of Pt_2O_4^+ . Energies, structures, and vibrational frequencies and IR intensities for all calculated isomers. This material is available free of charge via the Internet at <http://pubs.acs.org>.

■ AUTHOR INFORMATION

Corresponding Author

*E-mail: S.R.M., stuart.mackenzie@chem.ox.ac.uk; A.F., fielcke@fhi-berlin.mpg.de.

Notes

The authors declare no competing financial interest.

ACKNOWLEDGMENTS

We gratefully acknowledge the support of the Stichting voor Fundamenteel Onderzoek der Materie (FOM) in providing beam time on FELIX. We thank the FELIX staff for their skilful assistance, in particular Dr. A. F. G. van der Meer and Dr. B. Redlich. This work is supported by the Deutsche Forschungsgemeinschaft through research grant FI 893/3-1. D.J.H. acknowledges support from the Alexander-von-Humboldt-Stiftung.

REFERENCES

- (1) Gasteiger, H. A.; Kocha, S. S.; Sompalli, B.; Wagner, F. T. *Appl. Catal. B-Environ.* **2005**, *56*, 9–35.
- (2) Huber, G. W.; Iborra, S.; Corma, A. *Chem. Rev.* **2006**, *106*, 4044–4098.
- (3) Steininger, H.; Lehwald, S.; Ibach, H. *Surf. Sci.* **1982**, *123*, 1–17.
- (4) Gland, J. L.; Sexton, B. A.; Fisher, G. B. *Surf. Sci.* **1980**, *95*, 587–602.
- (5) Eichler, A.; Hafner, J. *Phys. Rev. Lett.* **1997**, *79*, 4481–4484.
- (6) Gambardella, P.; Šljivančanin, Ž.; Hammer, B.; Blanc, M.; Kuhnke, K.; Kern, K. *Phys. Rev. Lett.* **2001**, *87*, 056103.
- (7) Feibelman, P. J.; Hammer, B.; Norskov, J. K.; Wagner, F.; Scheffler, M.; Stumpf, R.; Watwe, R.; Dumesic, J. J. *Phys. Chem. B* **2001**, *105*, 4018–4025.
- (8) Hu, Q. M.; Reuter, K.; Scheffler, M. *Phys. Rev. Lett.* **2007**, *98*, 176103.
- (9) Heiz, U.; Sanchez, A.; Abbet, S.; Schneider, W.-D. *J. Am. Chem. Soc.* **1999**, *121*, 3214–3217.
- (10) Shi, Y.; Ervin, K. M. *J. Chem. Phys.* **1998**, *108*, 1757–1760.
- (11) Hermes, A. C.; Hamilton, S. M.; Cooper, G. A.; Kerpál, C.; Harding, D. J.; Meijer, G.; Fielicke, A.; Mackenzie, S. R. *Faraday Discuss.* **2012**, DOI: 10.1039/C2FD20019H.
- (12) Adlhart, C.; Uggerud, E. *Chem. Commun.* **2006**, 2581–2582.
- (13) Harding, D. J.; Kerpál, C.; Meijer, G.; Fielicke, A. *Angew. Chem., Int. Ed.* **2012**, *51*, 817–819.
- (14) Adlhart, C.; Uggerud, E. *Chem.—Eur. J.* **2007**, *13*, 6883–6890.
- (15) Balteanu, I.; Balaj, O. P.; Beyer, M. K.; Bondybey, V. E. *Phys. Chem. Chem. Phys.* **2004**, *6*, 2910–2913.
- (16) Schmidt, J.; Stuhlmann, C.; Ibach, H. *Surf. Sci.* **1993**, *284*, 121–128.
- (17) Feibelman, P. J.; Hafner, J.; Kresse, G. *Phys. Rev. B* **1998**, *58*, 2179–2184.
- (18) Jones, R. D.; Summerville, D. A.; Basolo, F. *Chem. Rev.* **1979**, *79*, 139–179.
- (19) Bare, W. D.; Citra, A.; Chertihin, G. V.; Andrews, L. *J. Phys. Chem. A* **1999**, *103*, 5456–5462.
- (20) Oepts, D.; van der Meer, A. F. G.; van Amersfoort, P. W. *Infrared Phys. Technol.* **1995**, *36*, 297–308.
- (21) Fielicke, A.; von Helden, G.; Meijer, G.; Simard, B.; Dénommée, S.; Rayner, D. M. *J. Am. Chem. Soc.* **2003**, *125*, 11184–11185.
- (22) Fielicke, A.; Meijer, G.; von Helden, G.; Pedersen, D. B.; Simard, B.; Rayner, D. M. *J. Phys. Chem. B* **2004**, *108*, 14591–14598.
- (23) Fielicke, A.; Kirilyuk, A.; Ratsch, C.; Behler, J.; Scheffler, M.; von Helden, G.; Meijer, G. *Phys. Rev. Lett.* **2004**, *93*, 023401.
- (24) Ahlrichs, R.; Bär, M.; Häser, M.; Horn, H.; Kölmel, C. *Chem. Phys. Lett.* **1989**, *162*, 165–169.
- (25) Tao, J.; Perdew, J. P.; Staroverov, V. N.; Scuseria, G. E. *Phys. Rev. Lett.* **2003**, *91*, 146401.
- (26) Weigend, F.; Häser, M.; Patzelt, H. *Chem. Phys. Lett.* **1998**, *294*, 143–152.
- (27) Weigend, F.; Ahlrichs, R. *Phys. Chem. Chem. Phys.* **2005**, *7*, 3297–3305.
- (28) Harding, D. J.; Kerpál, C.; Rayner, D.; Fielicke, A. *J. Chem. Phys.* **2012**, *136*, 211103.
- (29) Fielicke, A.; Gruene, P.; Haertelt, M.; Harding, D. J.; Meijer, G. *J. Phys. Chem. A* **2010**, *114*, 9755–9761.
- (30) Xu, Y.; Shelton, A. S.; Schneider, W. F. *J. Phys. Chem. A* **2006**, *110*, 5839–5846.
- (31) Wales, D. J.; Doye, J. P. K. *J. Phys. Chem. A* **1997**, *101*, 5111–5116.
- (32) Asmis, K. R.; Wende, T.; Brümmer, M.; Gause, O.; Santambrogio, G.; Stanca-Kaposta, E. C.; Döbler, J.; Niedziela, A.; Sauer, J. *Phys. Chem. Chem. Phys.* **2012**, *14*, 9377–9388.
- (33) Asmis, K. R.; Sauer, J. *Mass Spectrom. Rev.* **2007**, *26*, 542–562.
- (34) Wang, X.; Andrews, L. *J. Phys. Chem. A* **2001**, *105*, 5812–5822.
- (35) Lv, L.; Wang, Y.; Wang, Q.; Liu, H. *J. Phys. Chem. C* **2010**, *114*, 17610–17620.
- (36) Błoński, P.; Dennler, S.; Hafner, J. *J. Chem. Phys.* **2011**, *134*, 034107.
- (37) Titmuss, S.; Wander, A.; King, D. A. *Chem. Rev.* **1996**, *96*, 1291–1305.
- (38) Nolan, P. D.; Lutz, B. R.; Tanaka, P. L.; Davis, J. E.; Mullins, C. B. *Phys. Rev. Lett.* **1998**, *81*, 3179–3182.
- (39) Valentini, P.; Schwartztruber, T. E.; Cozmuta, I. *Surf. Sci.* **2011**, *605*, 1941–1950.
- (40) Ge, Q.; Hu, P.; King, D. A.; Lee, M.-H.; White, J. A.; Payne, M. C. *J. Chem. Phys.* **1997**, *106*, 1210–1215.
- (41) Nolan, P. D.; Wheeler, M. C.; Davis, J. E.; Mullins, C. B. *Acc. Chem. Res.* **1998**, *31*, 798–804.
- (42) Titov, A. V.; Jagodziński, H. *Surf. Sci.* **1985**, *152*, 409–418.
- (43) Lide, D. R. *CRC Handbook of Chemistry and Physics*, 76th ed.; CRC Press: Boca Raton, FL, 1995–1996.
- (44) Ackermann, M. D.; Pedersen, T. M.; Hendriksen, B. L. M.; Robach, O.; Bobaru, S. C.; Popa, I.; Quiros, C.; Kim, H.; Hammer, B.; Ferrer, S.; et al. *Phys. Rev. Lett.* **2005**, *95*, 255505.